A multidiagnostic investigation of the mesospheric bore phenomenon

Steven M. Smith,[1] Michael J. Taylor,[2] Gary R. Swenson,[3] Chiao-Yao She,[4]
Wayne Hocking,[5] Jeffrey Baumgardner,[1] and Michael Mendillo[1]

[1] Imaging measurements of a bright wave event in the nighttime mesosphere were made on 14 November 1999 at two sites separated by over 500 km in the southwestern United States. The event was characterized by a sharp onset of a series of extensive wavefronts that propagated across the entire sky. The waves were easily visible to the naked eye, and the entire event was observed for at least $5\frac{1}{2}$ hours. The event was observed using three wide-angle imaging systems located at the Boston University field station at McDonald Observatory (MDO), Fort Davis, Texas, and the Starfire Optical Range (SOR), Albuquerque, New Mexico. The spaced imaging measurements provided a unique opportunity to estimate the physical extent and time history of the disturbance. Simultaneous radar neutral wind measurements in the 82 to 98 km altitude region were also made at the SOR which indicated that a strong vertical wind shear of 19.5 $ms^{-1}km^{-1}$ occurred between 80 and 95 km just prior to the appearance of the disturbance. Simultaneous lidar temperature and density measurements made at Fort Collins, Colorado, ~1100 km north of MDO, show the presence of a large (~50 K) temperature inversion layer at the time of the wave event. The observations indicated that the event was most probably due to an undular mesospheric bore, a relatively uncommon disturbance which has only recently been reported [*Taylor et al.*, 1995a]. Evidence is also shown to suggest that a large east-west tropospheric frontal system lying over the northern United States was the origin of the disturbance.   *INDEX TERMS:* 0310 Atmospheric Composition and Structure: Airglow and aurora; 3332 Meteorology and Atmospheric Dynamics: Mesospheric dynamics; 3384 Meteorology and Atmospheric Dynamics: Waves and tides; 0394 Atmospheric Composition and Structure: Instruments and techniques; *KEYWORDS:* Airglow, waves, bore, mesosphere, dynamics, imaging

1. Introduction

[2] Multiwavelength all-sky imaging of the nighttime mesospheric emission layers can yield valuable vertical information about the structure and dynamics of the mesospheric region. Wave structures occur very frequently in these layers and have been shown to consist of at least two main types: bands [*Taylor et al.*, 1987] and smaller-scale ripples (<10 km) [*Peterson*, 1979; *Taylor and Hill*, 1991]. The band-type structures are believed to be due mainly to freely propagating and ducted internal atmospheric gravity wave (AGW) propagation through the layers [*Isler et al.*, 1997; *Walterscheid et al.*, 1999]. Such wave activity occurs ~50–60% of the time [*Taylor et al.*, 1997; *Smith et al.*, 2000]. The structures are usually very faint and well below visual detection. On rare occasions, however, wave events become visible to the naked-eye [*Peterson*, 1979; *Armstrong*, 1982; *Taylor et al.*, 1987]. These events appear to be associated with the so-called "Bright Night" phenomenon, a nonauroral enhancement of the nightglow emission [*Bates*, 1960; *Armstrong*, 1982]. Here we present measurements of an unusual naked-eye wave event that was observed in the nighttime mesospheric $O(^1S)$, Na and OH emission layers during the night of 13/14 November 1999 over the southwestern United States. The event consisted of a series of extensive light and dark bands which stretched across the entire sky from east to west and propagated southward from horizon to horizon.

[3] We present multidiagnostic (optical and radar) measurements that indicate that the disturbance was the result of a relatively uncommon type of wave in the mesosphere called an internal undular bore [*Dewan and Picard*, 1998].

[1]Center for Space Physics, Boston University, Boston, Massachusetts, USA.
[2]Space Dynamics Laboratory and Physics Department, Utah State University, Logan, Utah, USA.
[3]Department of Electrical and Computer Engineering, University of Illinois, Urbana, Illinois, USA.
[4]Physics Department, Colorado State University, Fort Collins, Colorado, USA.
[5]Department of Physics and Astronomy, University of Western Ontario, London, Ontario, Canada.
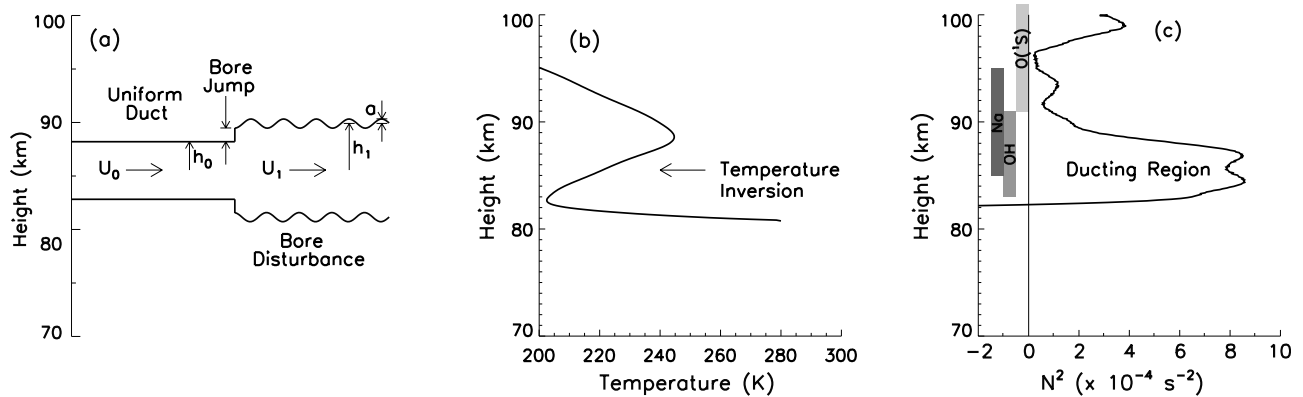
Figure 1. (a) Schematic diagram of an undular mesospheric propagating with a speed of U_0 within a ducting region. The frame of reference is stationary with respect to the bore. The undisturbed depth of the duct is h_0 and the disturbance results in an increased depth of h_1. The wave amplitude, a, is also shown. The wind flow is from left to right into the bore. The undulations at the top and bottom of the layer are 180° out of phase and are the cause of the complementary intensity variations observed between height-separated emission layers. (b) A 30-minute mean temperature profile obtained by the CSU Na lidar on 14 November 1999 at 0545 UT (discussed in detail later). A large 50K temperature inversion can be seen centered near 86 km. (c) Profile of the square of the Brunt-Vaisala frequency derived from the temperature profile in Figure 1b and using the dispersion equation for a windless atmosphere. A resulting ducting region with a FWHM of 6 km, occurs centered near 86 km. The three emission layers ($O(^1S)$, Na and OH) and their respective thicknesses are also shown. For comparison purposes, Figures 1a–1c have the same vertical scale.

These measurements are particularly important for several reasons:

1. It was the first mesospheric bore visible to the naked eye, as well as at multiple sites.

2. The first evidence of a co-located temperature inversion and of the sequential production of waves behind an undular bore as predicted by *Dewan and Picard* [1998].

3. The first explicit suggestion of the source of the bore.

[4] The word *bore* comes from the Medieval English word *bare* meaning *wave*. Traditionally, a bore, also known as an aegre, is a large wave-crest or series of wave-crests that travel upstream into a river or tidal estuary as the result of a tidal surge. Examples of estuarine bores include the Severn River bore, the largest in the UK [*Lighthill*, 1978], the Aragauri and Rio Gauna bores in Brazil, and the Hangzhou bore on the Qiantang river in China [*Simpson*, 1987]. The latter two can reach heights of 6 m (*Bore Riders Club*, 2001 (http://www.boreriders.com)). Bores have also been frequently observed in the lower troposphere [e.g., *Clarke et al.*, 1981; *Smith*, 1988; *Mahapatra et al.*, 1991]. The "morning glory," a traveling wave-cloud system in northern Australia, is one particular example [*Smith*, 1988].

[5] Bores have only recently been observed in the mesosphere [*Taylor et al.*, 1995a] and they were first identified as such by *Dewan and Picard* [1998] who investigated the Taylor et al. event. They developed a simple linear model for bore propagation in the mesosphere and estimated several parameters, such as the amplitude and the energy dissipation rate. Their follow-up paper [*Dewan and Picard*, 2001] suggested that mesospheric bores may occur as the result of a gravity-wave/critical-layer interaction with the mean wind flow and that both the resulting inversion layer and the bore share a common origin. *Munasinghe et al.* [1998] suggested that the same wave event could be explained by the interaction of two tidal modes within a ducting region but this explanation fails to explain the sudden emission increase just prior to the wave train or the emission intensity complementarity exhibited by the wave patterns in the nightglow layers during such events. Another similar event was reported by *Swenson and Espy* [1995]; their so-called "wall" event was interpreted as being the leading edge of a large internal gravity wave [*Swenson et al.*, 1998] whose passage rendered the local medium super-adiabatic. The resulting turbulence and heating produced an enhancement in the Na emission intensity.

2. Bores and Hydraulic Jumps

[6] The theory of bore formation and propagation in rivers and oceans is relatively well-understood [e.g., *Rayleigh*, 1908; *Lamb*, 1932; *Lighthill*, 1978]. For an incompressible fluid (see Figure 1a), the volume flux Q per unit width is constant, i.e., mass is conserved and $Q = U_0 h_0 = U_1 h_1$, where U_0 and U_1 is the fluid speed relative to the bore before and after its passage, respectively. The parameter,

$$\beta = \frac{h_1 - h_0}{h_0} \qquad (1)$$

known as the normalized bore strength [*Lighthill*, 1978] describes the ratio of the depth behind the jump (h_1) to the depth prior to it (h_0). A net loss of energy occurs across the hydraulic jump. This energy is transmitted backward from the jump and, if $\beta < 0.3$, results in the creation of a series of trailing wavefronts. The waves are phase-locked to the step and propagate along the stable layer. This disturbance is called an undular bore. When $\beta > 0.3$, the waves will break and the bore will consist of propagating jump with a trailing region of turbulence, sometimes called a foaming bore. Energy may also be lost by leakage from the ducting region.

[7] Recently, *Dewan and Picard* [1998] developed a simple model for internal bore propagation in the mesosphere from surface bore theory. For a weak bore ($\beta \ll 1$) producing long waves in a shallow medium, the velocity (U), horizontal wavelength (λ_h), and amplitude (a) of an internal bore is dependent on the width of the inversion layer ($2h_0$) by the relationships

$$U = U_0 = \sqrt{g' \frac{h_1(h_1 + h_0)}{2h_0}} \qquad (2)$$

$$\lambda_h = \frac{2\pi h_1}{3} \sqrt{\frac{2h_0}{h_1 - h_0}} \qquad (3)$$

$$a = \frac{1}{\sqrt{3}} \frac{h_1(h_1 - h_0)}{h_0} \qquad (4)$$

[8] The parameter g' is the acceleration due to gravity corrected for buoyancy, such that $g' = g \frac{\Delta\phi}{\phi}$, where ϕ is the mean potential temperature at the bore altitude and $\Delta\phi$ is the change in potential temperature from h_0 to h_1. This relation replaces the density factor in surface bore theory (see *Dewan and Picard* [1998] for more details).

[9] To relate the geometry of Figure 1a, showing a simple mesospheric bore propagating on a stable layer, such as a duct, to aeronomic parameters on the same height scale, Figure 1b shows a temperature profile with an inversion occurring in the 82 to 89 km height region. The corresponding height profile of the square of the Brunt-Vaisala frequency (N^2) (deduced from the dispersion equation for a windless atmosphere) is shown in Figure 1c. A ducting region arising from the temperature inversion can be seen to occur between 82 and 89 km. The nominal height regions of the three mesospheric emissions due to O(^{1}S), Na and OH are also shown.

[10] For a bore disturbance with a horizontal wavelength λ_h and amplitude a, propagating on a stable layer of mean depth h, the quantity

$$c_n = \frac{a\lambda_h^2}{h^3} \qquad (5)$$

is a measure of the amount of nonlinearity associated with the wave disturbance. When this parameter is zero, the waves are sinusoidal. As the parameter increases, the waves exhibit crest widths which become increasingly more narrow compared to the corresponding trough widths. These weakly nonlinear wave forms are known as cnoidal waves – a family of elliptic solutions to the nonlinear wave equation [*Drazin and Johnson*, 1989]. As c_n increases further (to $\sim$16) the bore becomes a train of strongly nonlinear solitary waves (solitons). For $c_n > 16$, the wave breaks and turbulence is created.

3. Imaging Observations

[11] Imaging observations were made on the night of 13/14 November 1999 using three bare charge-coupled device (CCD) wide-angle imaging systems at two sites: (1) the Boston University field station at McDonald Observatory (MDO), Fort Davis, Texas (30.67°N, 104.02°W) (all-sky imager in O(^{1}S), Na and OH emission) and (2) the Starfire

Optical Range (SOR) near Albuquerque, New Mexico (34.93°N, 106.46°W), approximately 530 km to the northwest of MDO (all-sky imager in OH and a wide-field (75°) OH Mesospheric Temperature Mapper). These imaging systems have been described previously (*Baumgardner et al.* [1993], *Swenson and Mende* [1994], and *Taylor et al.* [1999], respectively). The MDO and SOR imaging measurements provided an excellent opportunity to observe the disturbance over a large area and for a substantial period of time, allowing a comprehensive determination of the time history of the disturbance. The imaging measurements were complemented with simultaneous temperature and density profile measurements of the Na layer from the Colorado State University (CSU) Na resonance scattering lidar sited at Fort Collins, Colorado (40.59°N, 105.14°W) [*She et al.*, 1991; *Yu and She*, 1995], and with simultaneous meteor radar wind measurements from the 85 to 95 km height region obtained by the All-Sky Interferometric Meteor Radar (SKiYMET) at the SOR. The relative locations of the instruments are shown in Figure 2.

[12] The CSU Na resonance lidar actively samples the Na layer in the 70–110 km height region. The technique exploits the large resonance cross-section of Na in which incident 589 nm photons are absorbed and then rapidly re-emitted with no loss of energy. The lidar transmits pulses at three selected frequencies within the Doppler-broadened width of the Na D2 transition at 589 nm and records the back-scattered emission at each frequency separately. By normalizing the scattered photons to Rayleigh scattering and standard air density at a lower height, typically at 30 km, the data can be inverted to produce a vertical profile of Na densities and temperatures without other adjustment, i.e., from the first principle of quantum mechanics on Na atoms. Measurements were made every three minutes and the profiles were combined into 30-minute bins in order to increase the signal-to-noise ratio.

[13] At MDO, the visual appearance of the "bright wave" event was characterized by a sharp frontal onset followed by a series of extensive bright and dark bands that covered the entire sky. Figure 3 shows four raw all-sky images during the event from MDO in (a) 557.7 nm (O(^{1}S)), (b) 589.3 nm (Na), (c) 769.9 nm (P_1(6) doublet of OH(4-0) band), and (d) 644.4 nm (offband) emission. The bright bands were comparable in brightness to the Milky Way. A complementarity between the O(^{1}S) and Na and the OH intensity variations, similar to that reported by *Taylor et al.* [1995a], can be seen in the images. Sky conditions were excellent and the post-midnight event continued for over two hours until dawn light halted observations. The 557.7 nm wave amplitudes were greater than the 589.3 nm amplitudes and, in both emissions, the first dark band exhibited the greatest amplitude, with the amplitudes decreasing with distance from the beginning of the train.

[14] As part of our analysis, the all-sky images were unwarped, i.e., geometrically corrected for lens distortion, and then mapped down onto the Earth's surface for assumed layer heights of 90 km (Na) [*Newman*, 1988] and 96 km (O(^{1}S)) [*Donahue et al.*, 1973]. Figure 4 shows two time series (time increasing downward) of unwarped all-sky images in (a) 557.7 nm and (b) 589.3 nm emission from MDO. The images have also been corrected for vignetting by the optical system and for line-of-sight viewing effects,
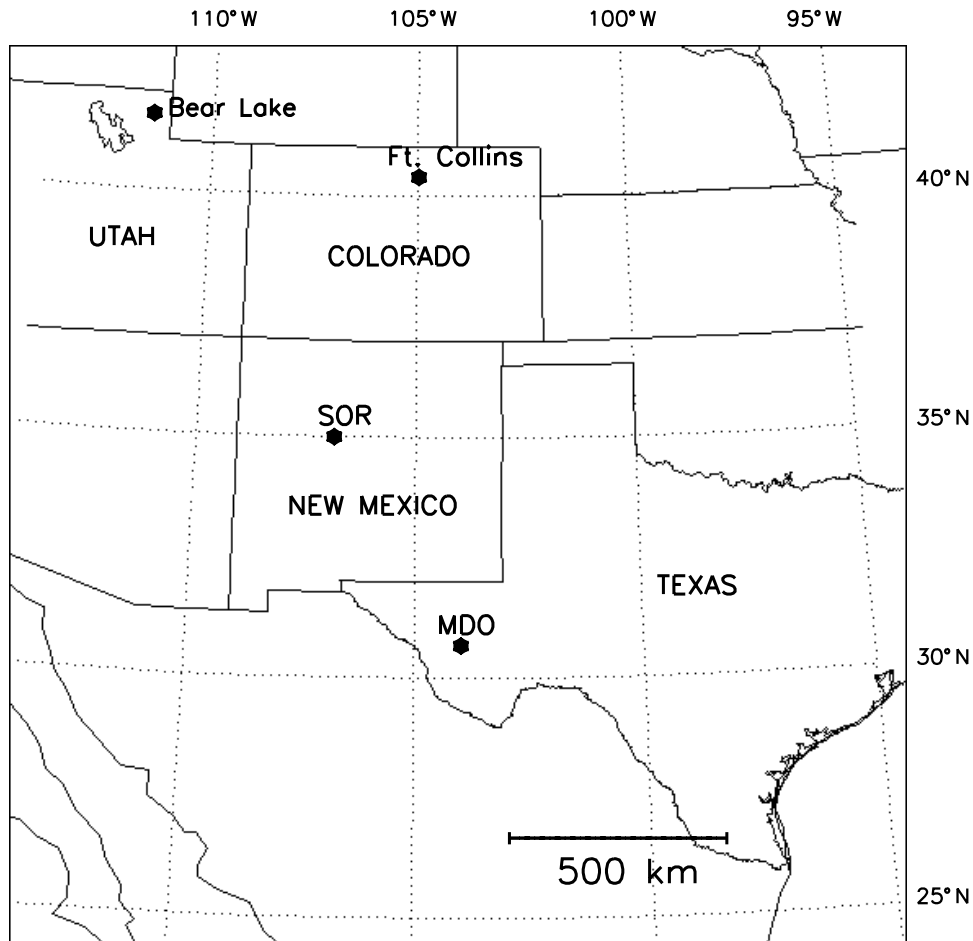
Figure 2. Map showing the relative locations of imaging and lidar systems used in this study. The spaced optical measurements provided evidence of a large wave event that traveled over 1200 km southward from beyond northern Colorado into Mexico and lasted over seven hours.

such as van Rhijn brightening near the horizon. North is at the top of each panel and east is to the right. The relative positions of MDO and the SOR are indicated.

[15] The large horizontal extent of the wave pattern is clearly evident in Figure 4 with the leading wavefront being the widest, stretching approximately 950 km from east to west. The trailing wavefronts were approximately 400–600 km wide. The entire length of the wave system was greater than the MDO imager's field of view, 1000 km at 96 km. The lack of curvature of the wavefronts indicated that the disturbance originated from either (i) an extended source, such as a tropospheric front or a jet stream, that was aligned near E-W or (ii) a localized source, such as a convection center, that was situated at a much larger distance ($\gg$1000 km) from MDO.

[16] The disturbance was first detected in the SOR images at 0708 UT low on the northern horizon and it passed through zenith at 0844 UT. Figure 5 shows a time-differenced image (used to increase the contrast) [*Swenson and Mende*, 1994] of the event in OH emission taken by the all-sky imager at the SOR at 0908 UT. The leading edge of the disturbance at this time can be seen near the southern horizon extending from east to west and followed by a series of wavefronts. The event was first detected in all-sky images at MDO at 0956 UT low on the northern horizon.

The disturbance passed through zenith at 1052 UT and was tracked into the dawn twilight until 1235 UT. The dual observations indicate that the lifetime of the disturbance was at least $5\frac{1}{2}$ hours during which time the leading edge of the disturbance traveled over 1200 km. At MDO, the event was visible to the naked eye from about 1000 UT to 1130 UT. There were no observers at the SOR so the total period of naked-eye visibility is unknown.

[17] Initially, at the SOR, the propagation direction was southeastward (azimuth 165–170°N), but it had rotated around to about 180° by the time it was observed at MDO. The direction continued to change clockwise and reached about 195° at dawn. This rotation can be seen clearly in the later MDO images in Figure 4 and was probably caused by variations (temporal and/or spatial) in the wind field or the duct during the period.

[18] Several images in the near-infrared (NIR) sky emission, at 769.9 nm (FWHM = 1.4 nm) and 765.0 nm (FWHM = 1.4 nm)), were also obtained during the event at MDO. The 769.9 nm filter transmits the $P_1(6)$ doublet of the OH(4-0) Meinel band and the 765.0 nm filter transmits the $P_2(5)$ line from the same band. The wave structure in the NIR images is approximately 180° out of phase with that in the 557.7 nm and 589.3 nm images, which is identical to the relative phases reported by *Taylor et al.*

(a) O(^{1}S) 557.7 nm   10:45:32 UT
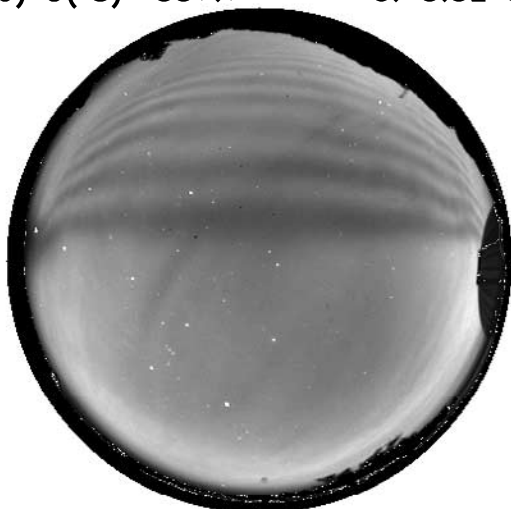
(b) Na 589.3 nm   10:42:03 UT
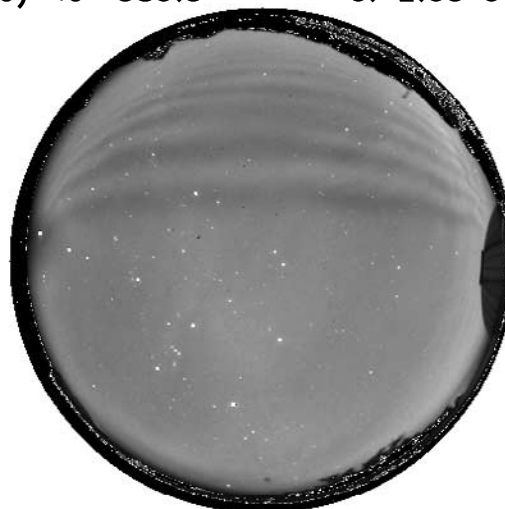
(c) OH 769.9 nm   12:16:29 UT
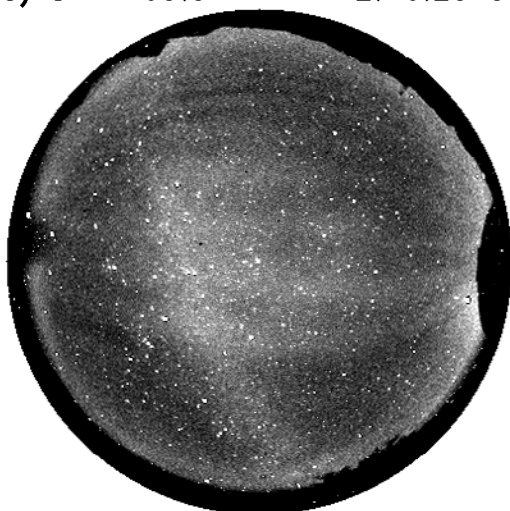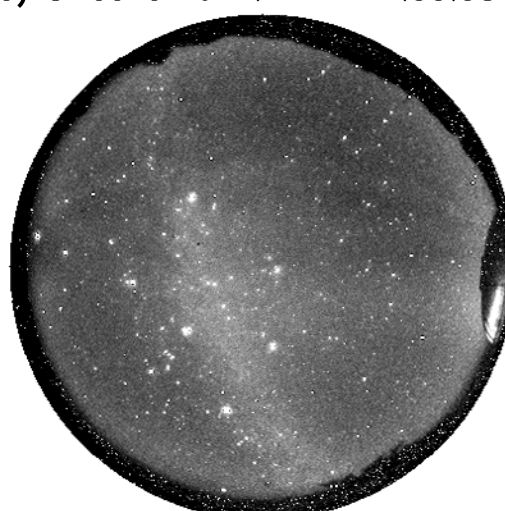
(d) Offband 644.4 nm 11:33:58 UT

Figure 3. Four raw all-sky images during the bright wave event over McDonald Observatory in (a) 557.7 nm emission (O(^{1}S)), (b) 589.3 nm emission (Na), (c) 769.9 nm emission (OH), and (d) 644.4 nm emission (offband). The complementarity of the wave intensity structure between the O(^{1}S) and Na images and the OH image is clearly evident. Two bright wavefronts can be faintly discerned in the upper half of the offband image (Figure 3d).

[1995a]. Emission due to mesospheric potassium, which occurs at a similar height to the Na layer (90 km [*Eska et al.*, 1998]), is possible in the 769.9 nm images but the emission brightness is normally only ~1 R or less [*Slanger and Osterbrock*, 2000], much less than the expected OH contribution. Also, the wave structure in the images at both NIR wavelengths is in phase and spatially coherent so we attribute the NIR wave structure in the 769.9 nm images to OH emission near 87 km.

4. Data Analysis

[19] The 557.7 and 589.3 nm and offband zenith sky brightnesses at MDO on the night of 13/14 November 1999

(a) O(^{1}S) 557.7 nm
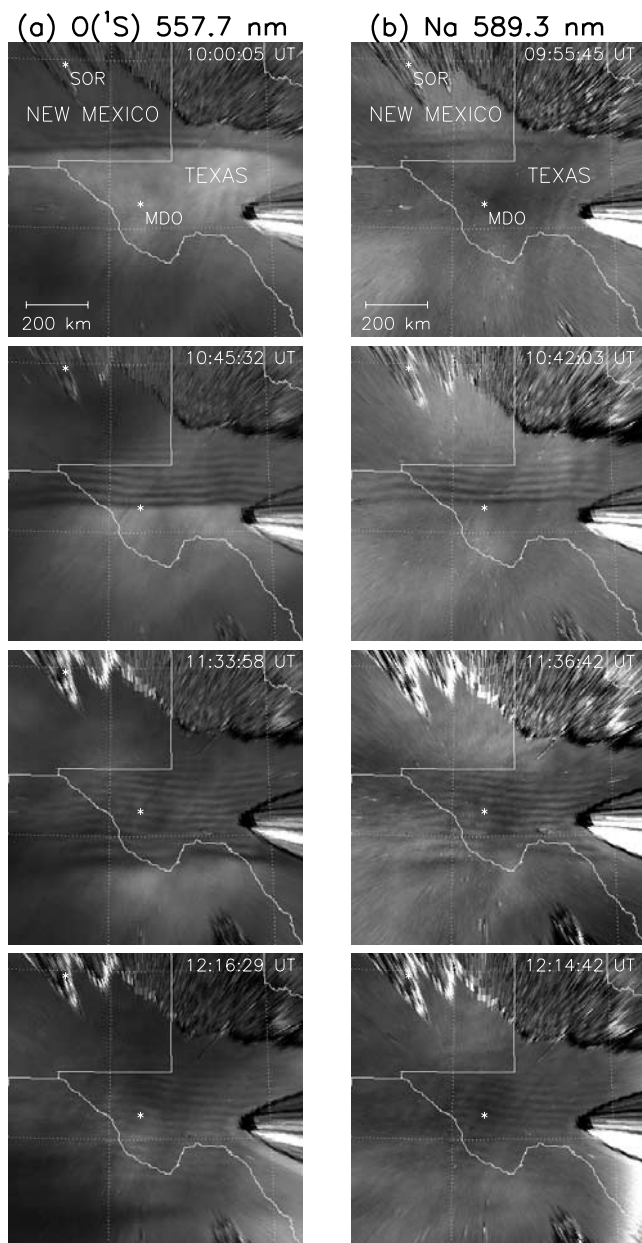

(b) Na 589.3 nm

Figure 4. Two time series of unwarped all-sky images in (a) 557.7 nm and (b) 589.3 nm emission. North is at the top of each panel and east is to the right. Time is increasing downward. The large conical shape in the east is the observatory dome and the dark shape along the northern horizon is the summit of Mt. Locke. The outlines of the states of Texas and New Mexico are shown, including the relative positions of McDonald Observatory (MDO) and the Starfire Optical Range (SOR). The large horizontal extent and temporal evolution of the wave event are clearly evident.

are shown in Figure 6. Each point represents a sampled zenith area of $1.2° \times 1.2°$ (2 km $\times$ 2 km at 96 km). The disturbance consisted of a large-scale brightness increase followed by a sudden onset of a series of trailing smaller scale waves. Several hours prior to the event (6–8 UT), the 557.7 and 589.3 nm brightnesses were 350–400 R and 200–250 R, respectively. The appearance of the wave train

over the northern horizon at MDO coincided with a more than two-fold increase (to ~750 R) in the zenith 557.7 nm emission intensity. But, as the leading wavefront passed through zenith, the 557.7 nm emission suddenly decreased back almost to the level during the early part of the night (6–8 UT). Prior to the wave train's arrival, the 589.3 nm zenith emission increased only slightly, but it increased to ~400 R during the passage of the small-scale waves, opposite to the corresponding 557.7 nm emission behavior.

[20] The image acquisition rate allowed the detection (see Figure 6) of only the gross brightness variations associated with the wave event and the individual wavefronts were not resolved. However, visual inspection of the images indicated that the observed differences between the 557.7 and 589.3 nm intensities in Figure 6 were real. During the preceding night (12/13 November), the 557.7 nm emission varied between 340 R and 450 R but the presence of thin cirrus cloud may have contributed to these elevated levels by increasing the amount of scattering of light from extraneous tropospheric and ground sources. The 557.7 nm emission on the night following the disturbance (14/15 November) ranged from 240 R to 330 R, lower than that exhibited on 14 November.

[21] The off-band sky brightness (644.4 nm) remained constant throughout the entire night at ~70 R but there was a slight increase of ~10 R around the time of zenith passage of the beginning of wave train (at ~1050 UT). During this time, the leading 2 to 3 wavefronts were visible in subsequent offband images; taken at 1050 UT and 1130 UT (see Figure 3d). This time period coincided with time of the 557.7 nm enhancement and the period of naked-eye visibility at MDO. The offband filter was centered at 644.4 nm and had a passband (FWHM) of 1.4 nm so it is probable that the observed offband wave structure was due to an enhancement of the $P_2(7)$ doublet of the OH(9-3) Meinel band at 645.2 nm as a result of the disturbance. The gap in the time histories between 8–10 UT in Figure 6 was due to instrument calibration.

[22] Figure 7 shows the vertical cross-section of the wave train in the direction of propagation (denoted by the arrow) at similar times using unwarped image slices in the three emissions. The 589.3 nm (Na) and 769.9 nm (OH) image cross-sections have been shifted horizontally by 5 and 37 pixels (13 and 90 km), respectively, to correct for the time differences between these and the 557.7 nm image. The time differences resulted from the sequential acquisition of the images. The amount of shift was determined by the time difference between each image, and the velocity of the corresponding wavefronts. The velocity of each wavefront was found to be constant during the observing period, as discussed below.

[23] The amplitude of the leading wave in the 557.7 nm emission was about 50 R above the mean level (Figure 7). The large-scale brightening in the 557.7 nm emission prior to the wave-fronts was about 175 R above the mean emission level during the passage of the wavefronts. A brightening of ~100 R is also evident in the Na emission prior to the wave train (see also Figure 7) but it is smaller than in the 557.7 nm emission. The disturbance appears to have reached the Na and OH layers first, followed by the O(^{1}S) layer about a minute later, but the OH emission variations were approximately 180° out-of-phase with those of the O(^{1}S) and Na
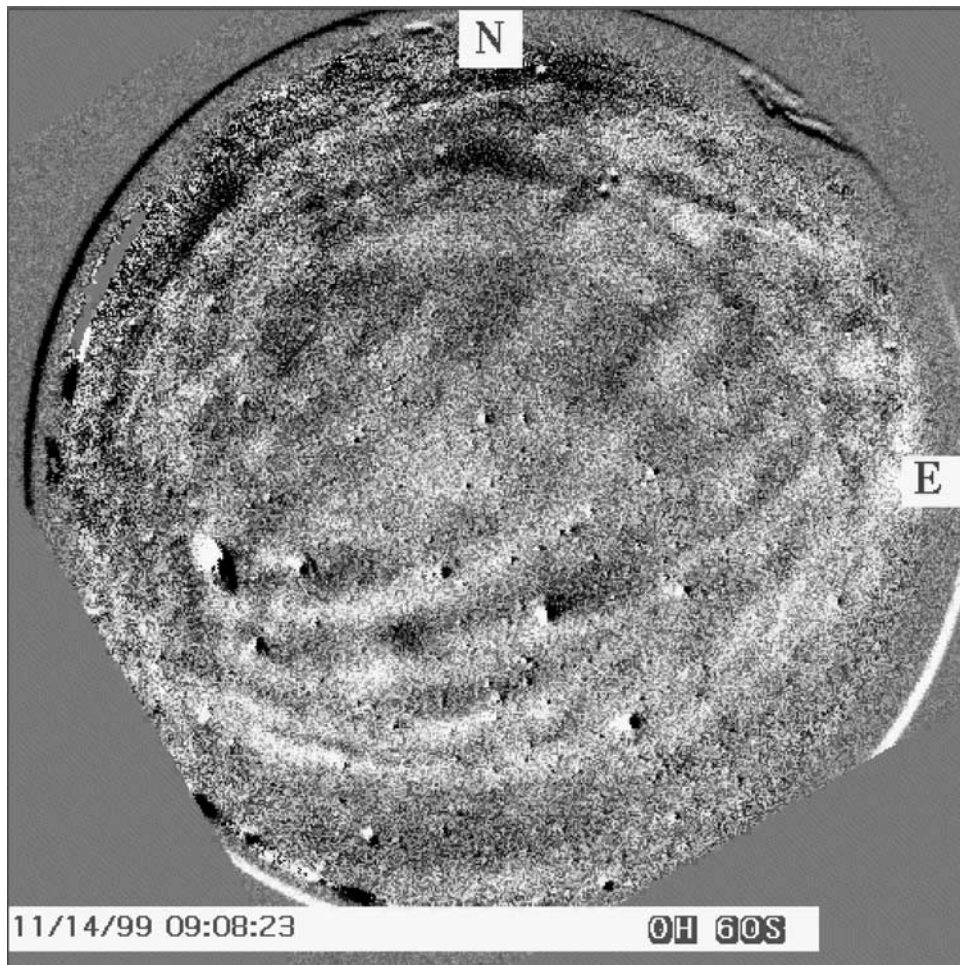
Figure 5. Time-difference all-sky image in OH emission of the wave disturbance recorded at the Starfire Optical Range on 14 November 1999 at 0908 UT. The image is the result of subtracting two subsequent images in order the increase the contrast of the wave structure in the image. The leading edge of the disturbance can be seen near the southern horizon extending from east to west and followed by a series of wavefronts.

layers, which is consistent with a bore-like disturbance moving through the region centered near 87 km.

[24] Figure 8a shows the time history of the pixel positions of the first fourteen light and dark wavefronts as measured from unwarped MDO 557.7 nm all-sky images. A total of at least seventeen dark wavefronts were observed to comprise the wave train at MDO before the dawn twilight halted observations. The linear least-square fits to each wavefront's position time history are also shown and they indicate that the individual waves each traveled at a constant velocity for at least 3 hours. The deduced speeds, derived from the slopes of the linear fits, are plotted in Figure 8b. The leading wavefronts are clearly traveling faster ($\sim$60 ms^{-1}) than the trailing wavefronts ($\sim$40 ms^{-1}). The uncertainty values shown are the uncertainties of the linear fits in Figure 8a. The solid line is the linear fit to the phase velocities of both the light and dark wavefronts. The leading wavefront propagated with an average speed of 60.2 $\pm$ 0.6 ms^{-1}. The observed period associated with the leading waves was approximately 8.0 minutes. At 1100 UT, the intrinsic period was 5.4 minutes, which is very close to, or at, the Brunt-Vaisala period of natural oscillation in the mesosphere.

[25] The wavefronts also exhibit evidence of amplitude ordering, i.e., the leading wavefront exhibited the largest amplitude. The speed distribution between wavefronts is a nonlinear consequence of amplitude ordering [*Lamb*, 1932; *Christie*, 1989]. Such behavior has been reported previously, in association with a tropospheric bore [*Mahapatra et al.*, 1991]. Another consequence of the nonlinear behavior was that the distances between successive wavefronts increased with time. The average spacing between each wavefront was 30.2 km. Furthermore, at any fixed time, the spacing between successive wavefronts decreased with increasing distance from the leading wavefronts. *Dewan and Picard* [1998] described an almost identical event [*Taylor et al.*, 1995a] that exhibited fewer wave crests but that were all apparently phase-locked to, and traveling at the same speed as, the leading front.

[26] The zenithal intensity time history of the P$_1$(2) line emission in the OH(6-2) Meinel band at the SOR is shown in Figure 9a. It has the same form as the Na emission history at MDO (Figure 6), but at the SOR, a 20−25% enhancement in the OH emission occurred about 45 minutes after the leading wavefront crossed the zenith. The Na emission
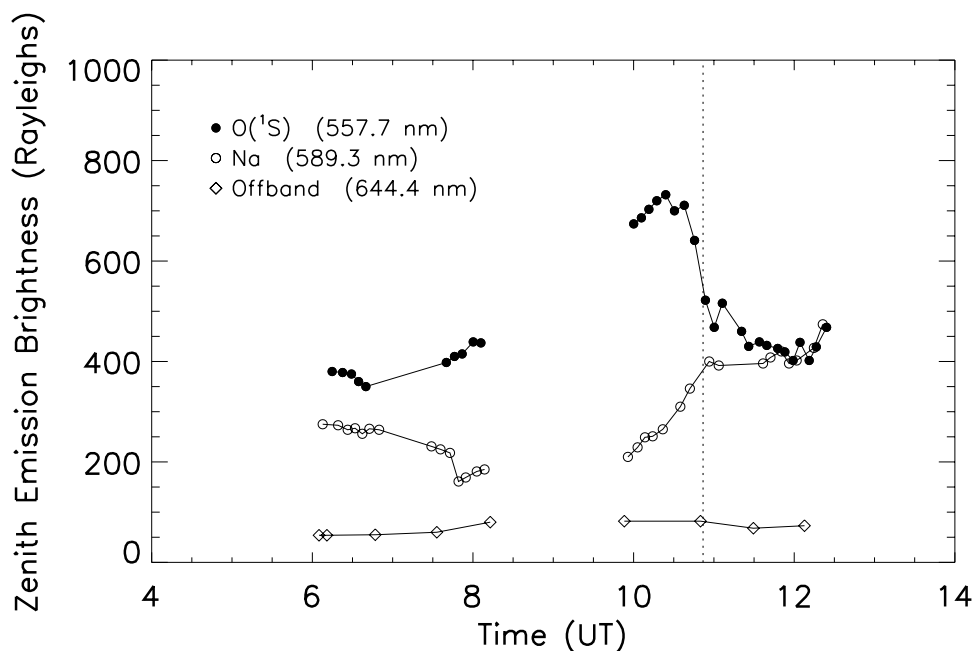
Figure 6. Zenith airglow brightness history at MDO during the night in the 557.7 and 589.3 nm emissions. The time when the center of the leading dark wavefront reached zenith is shown by the vertical dashed line. The brightness variations of each emission are clearly different. The 557.7 nm brightness decreased during the event but the 589.3 nm emission increased. The offband (644.4 nm) brightness remained essentially constant during the night. The gap in the history between 8–10 UT was due to calibration of the instrument.

enhancement at MDO occurred immediately after the leading wavefront crossed the zenith. It is uncertain why the OH emission enhancement at the SOR exhibited such a delay because, during the *Taylor et al.* [1995a] event, an OH emission enhancement occurred in unison with the leading wavefront crossing the zenith. Figure 9b shows the corresponding OH(6-2) rotational temperature at the SOR. The temperature prior to the event was about 190 K but a 4 K
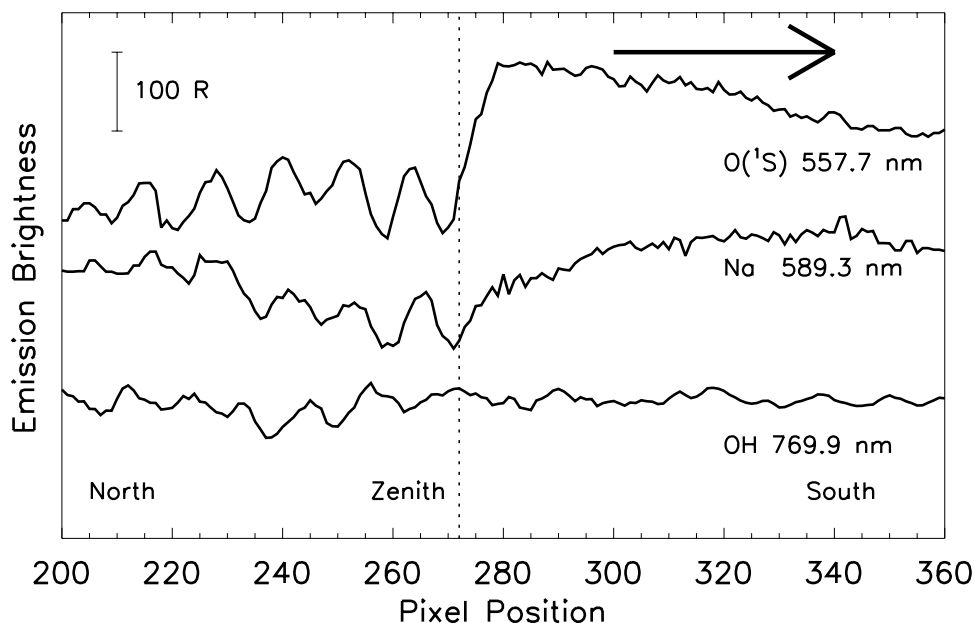

Figure 7. Plots of the brightness variations perpendicular to the wavefronts and through zenith from unwarped 557.7 nm (1045 UT), 589.3 nm (1042 UT) and 769.9 nm (1110 UT) images. The direction of motion (southward) is shown by the bold arrow. The 589.3 nm and 769.9 nm plots have been shifted to the right by 5 and 37 pixels (13 and 90 km), respectively, to correct for the time differences between the three observations. The 557.7 nm and 589.3 nm emission variations are clearly in phase but the 769.9 nm emissions are approximately 180° out of phase with the other two.
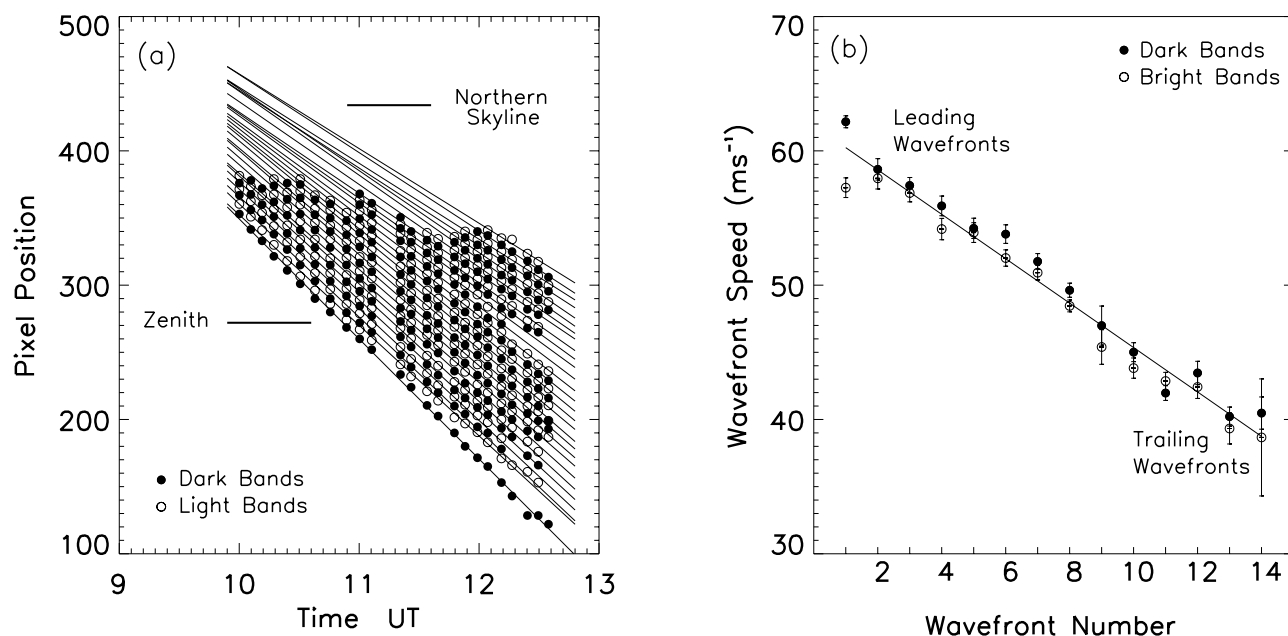
Figure 8.   (a) Time history of the leading fourteen light and dark wavefronts in the 557.7 nm emission at MDO as a function of pixel position. The solid lines denote the best linear fits to each wavefront position history. The positions of the northern skyline and the zenith are also marked as horizontal bars. The horizontal distance between each successive wavefront increases with time. (b) Propagation speeds of the leading fourteen light and dark wavefronts in the 557.7 nm emission shown in Figure 8a. The leading wavefronts are clearly traveling faster than the trailing ones. The solid line is the linear fit to the measured phase velocities of both the light and dark wavefronts.

increase occurred 45 minutes after the zenithal passage of the leading wavefront. A large 5 K temperature spike (shown in Figure 9b) also occurred about 20 minutes after the event began. The occurrence time of the spike coincided with the onset of the OH intensity enhancement.

[27]   Figures 10a and 10b show the full time history of the wave event from slices of the unwarped 557.7 and 589.3 nm images made perpendicular to the wavefronts. The pair is a more comprehensive series of cross-sections than shown for a "single time" in Figure 7 and they illustrate several important differences in the morphology of the wave between the two emissions. The 557.7 nm slices, in particular, show the large-scale brightness enhancement, followed by the series of small-scale ($\lambda_h \sim 30$ km) waves. These waves were phase-locked to the leading enhancement, similar to that seen in the *Taylor et al.* [1995a] event. The Na emission slices do not show such a large initial intensity enhancement but the wavefronts appear to be superimposed upon a larger amplitude (2 to 3-times) variation of longer period ($\sim$hours) and with a much larger horizontal scale size (300–400 km). The centroid height of the disturbance was below the $O(^1S)$ and Na layers (at $\sim$96 and $\sim$90 km, respectively) but slightly above the OH layer at $\sim$86 km.

5.   Radar Wind and Lidar Temperature Measurements

5.1.   Meteor Wind Observations

[28]   Figure 11 shows the 2-hourly mean neutral wind profiles between 82 and 98 km obtained by the SKiYMET meteor radar system [*Hocking et al.*, 2001] at the SOR on 14

November 1999. The uncertainty of each wind value is $\sim$5 ms^{-1}. A downward tidal phase progression of 1.5 km hr^{-1} (0.4 ms^{-1}) can clearly be seen in the meridional and zonal winds maxima. A large vertical wind shear of 19.5 ms^{-1}km^{-1} centered near 88 km can be seen to occur in the meridional winds at about 0700 UT (Panel a). Taking into consideration the calculated transit time of the disturbance between the SOR and MDO, the time of the wind shear maximum coincided with the observed 557.7 nm emission enhancement. At that time, the meridional wind near 96 km was southward. The zenithal passage of the wave train occurred immediately after the meridional wind changed to the north. Below 90 km, the meridional winds were initially strongly northward, but after the passage of the wave train they became weakly southward. The behavior strongly suggests that the tidally dominated wind field blocked the southward passage of the disturbance and its associated wind shear. A weak shear also occurred in the zonal winds at 0600 UT. This coincided with a separate, much fainter wave disturbance (not discussed in this paper) which was also seen in the SOR images propagating to the southwest.

[29]   At 0700 UT and 0900 UT, the Richardson Number (Ri, the criterion for dynamic instability) in the 85 to 94 km region was estimated to be near-zero, which suggests that the region was dynamically unstable prior to and during the passage of the disturbance over SOR. This was especially so during the occurrence of the wind shear. The 557.7 nm enhancement was probably the result of heating by turbulence due to the disturbance.

[30]   If, for a moment, we suppose that the disturbance was not a bore but a large freely propagating internal gravity
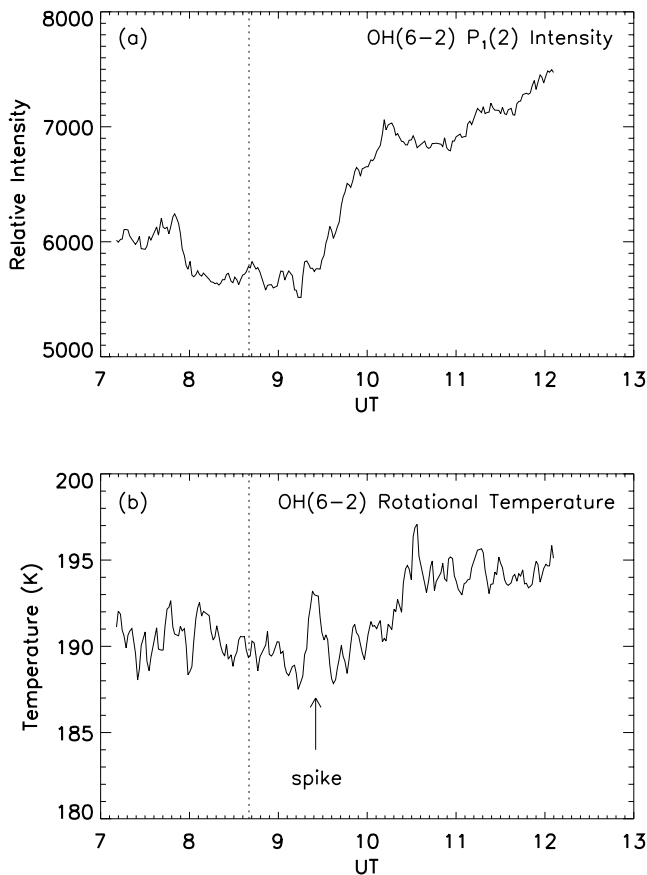
Figure 9. (a) Zenith airglow brightness history at the SOR of the $P_1(2)$ emission line of the OH(6-2) Meinel band. (b) History of the rotational temperature of the OH layer at the SOR. The vertical dashed line in each figure indicates the time at which the leading dark wavefront was at zenith.

wave, we can use the dispersion equation and the meteor winds to calculate a vertical wavelength (λ_z). For an isothermal, horizontally stratified atmosphere, where ω_b is the Brunt-Vaisala frequency, H is the atmospheric scale height ($\sim$6 km), c_{ob} is the observed phase speed of the wave, u is the magnitude of the mean wind in the direction of wave propagation, and m and k are the vertical and horizontal wavenumbers, respectively (where $m = 2\pi/\lambda_z$ and $l = 2\pi/\lambda_h$), the dispersion equation can be approximated to

$$\text{m}^2 = \frac{\omega_b^2}{\left(c_{ob} - u\right)^2} - k^2 - \frac{1}{4H^2} \tag{6}$$

[31] For this purpose, the neutral meridional winds in Figure 11a were averaged over two height ranges: 94 and 98 km winds (= 96 km), and 85 and 88 km winds (= 87 km), to better match the heights and thicknesses of the O(^{1}S) and OH emission layers, respectively. At 0900 UT, just after the beginning of the wave train passed over the SOR, the meridional winds at 96 km and 87 km were 1 ms^{-1} and 13 ms^{-1}, respectively, both southward. As a result, the intrinsic horizontal phase velocity of the wave would be 59 ms^{-1} and 47 ms^{-1}, respectively, and, using Equation (6), the vertical wavelength would be 26 km (O(^{1}S)) and 18 km (OH). Since, the O(^{1}S) and OH layers are nominally

separated by 10 km, such a wave with $\lambda_z \sim 22$ km would produce the observed complementary wave patterns. But, although the resultant horizontal phase speed and vertical wavelength are consistent with the disturbance being a large freely propagating internal gravity wave there are several other characteristics about this wave event which indicate that this is not the correct interpretation (as discussed in section 8).

5.2. Lidar Observations

[32] The number density of the mesospheric Na layer during the night of 14 November 1999 is shown as a contour plot in Figure 12a. The measurements were obtained with the CSU Na resonance lidar at Fort Collins, CO., approximately 1100 km directly north of MDO. The Na number density increased steadily during the night but increased suddenly by 15–20% after 0515 UT to a maximum of 8.3×10^9 m^{-3} near 87 km at 0600 UT. The density then decreased slowly during the following 1–2 hours. Assuming a constant phase speed for the bore of 60 ms^{-1} southward, the leading wavefront of the bore would have been located over the lidar site at 0555 UT (marked as a dashed vertical white line). The enhancement coincided with the deduced onset of the disturbance over the lidar site and also with the measured temperature increase. The Na emission rate is temperature sensitive so the 5 K temperature increase in the OH emission observed at the SOR during the passage of the disturbance would partly explain the observed Na brightness enhancement observed at MDO after the onset of the disturbance (Figure 6). The width of the Na layer also increased by a factor of two between 0400 and 0800 UT. The height of the maximum Na density steadily decreased at a rate of 0.2 ms^{-1} during the course of the night.

[33] Figure 12b is a contour plot of the Na layer temperature profile obtained by the CSU Na lidar. The plot was derived from 30-minute averaged temperature profiles and it indicates that a large ($\sim$50 K) temperature inversion occurred in the mesosphere in the early hours of 14 November. The inversion moved downward from $\sim$89 km to 83 km over the course of the next five hours with a speed of 1.5 km hour^{-1} (0.4 ms^{-1}) which was similar to downward speed of the wind maxima observed at the SOR. The 30-minute temperature profiles removed any temperature variations with time-scales similar to the waves seen in the all-sky images at MDO. The temperature maximum at the deduced onset time was at an altitude of 88.5 ± 0.5 km. The temperature of the entire layer decreased markedly to almost mean levels in about 30 minutes after the onset time (Figure 12b). In addition, between 0530–0630 UT, the temperature lapse rate in the 90 to 100 km height region temperature was near-adiabatic and so was at the limit of convective stability.

[34] Figure 12c shows a contour plot of the square of the Brunt-Vaisala frequency (N^2) profiles calculated from the above temperature profiles. Free wave propagation may only occur in regions where N$^2 > 0$. A narrow height region, or duct, of allowed free propagation occurred between 82 and 90 km (red contoured region) at about 0600 UT. The region was centered at 85.5 ± 0.5 km and had a FWHM of 6.0 km (= $2h_o$ in Figure 1a). The region between 90–97 km exhibited near-zero N^2 values indicating reduced wave propagation there. What is also interesting is
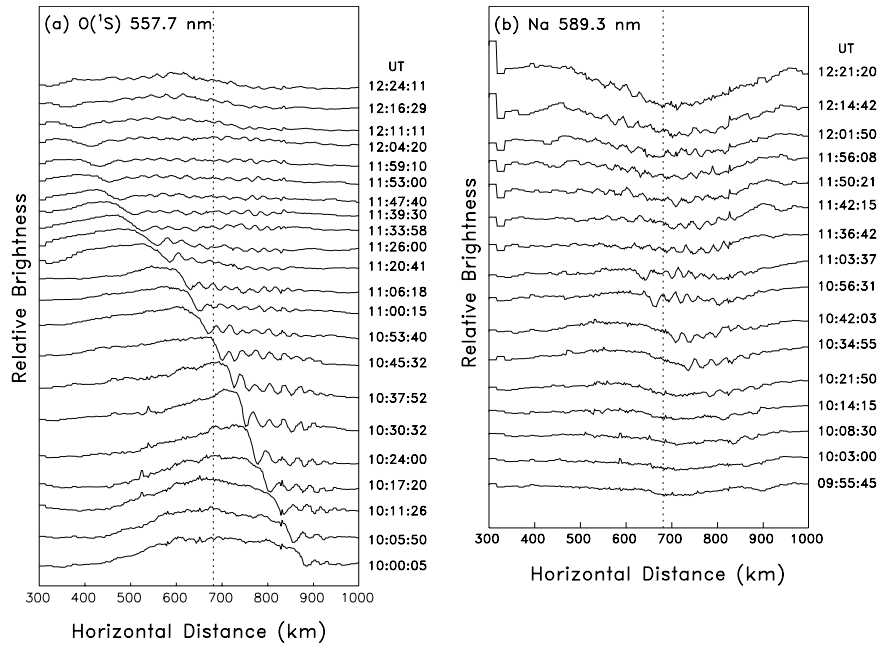
Figure 10. Slices through successive (a) 557.7 nm and (b) 589.3 nm unwarped emission images showing the time evolution of the wave event as it passed over MDO. The behavior of the wave in the two emissions is clearly different. The 557.7 nm images show a large intensity enhancement prior to the arrival of the wave train, this enhancement being the bore itself. The 589.3 nm images show the wave train superimposed upon a much larger-scale variation.
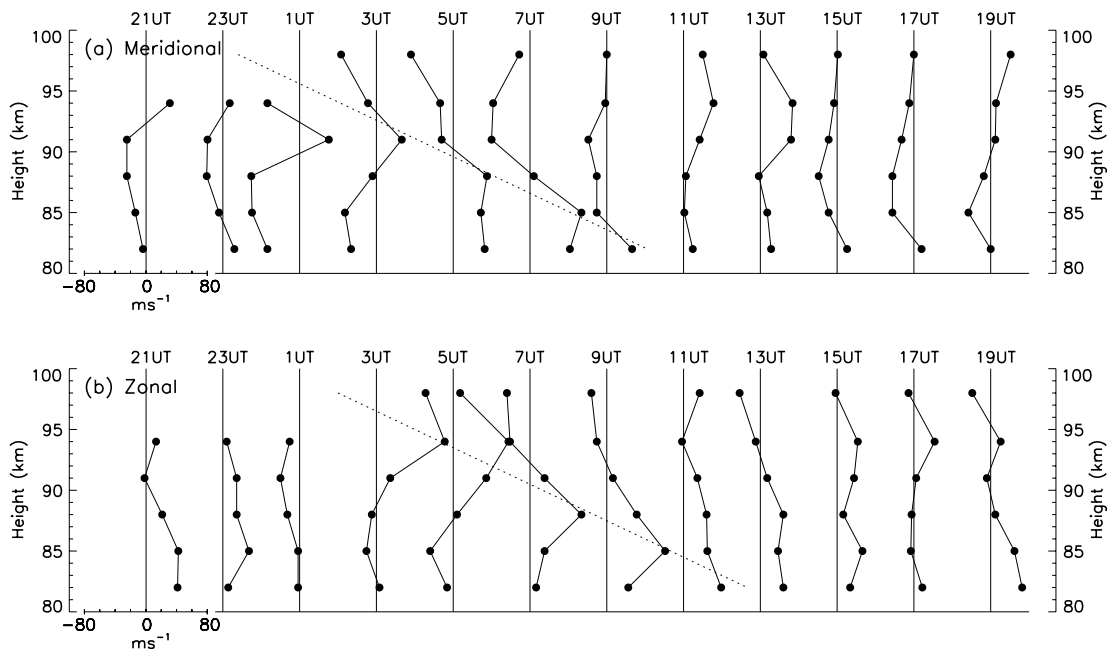

Figure 11. Vertical profiles of the (a) meridional and (b) zonal winds between 82 and 98 km obtained from the SKiYMET meteor radar at the Starfire Optical Range. A downward phase progression of 0.4 ms^{-1}, possibly of tidal origin, is evident in both components and denoted by the dotted lines. A large vertical wind shear of $\sim$19.5 ms^{-1} km^{-1}, centered near 87 km, in the meridional winds occurred during 0500−0700 UT. If allowance is made for the travel time of the disturbance between the SOR and MDO, the occurrence time of the shear coincided with the enhancement seen in the 557.7 nm night-glow at MDO. The zenithal passage of the wave train occurred just after the shear ended, when the meridional winds were near-zero and becoming northward (at $\sim$0845 UT) (Figure 11a).
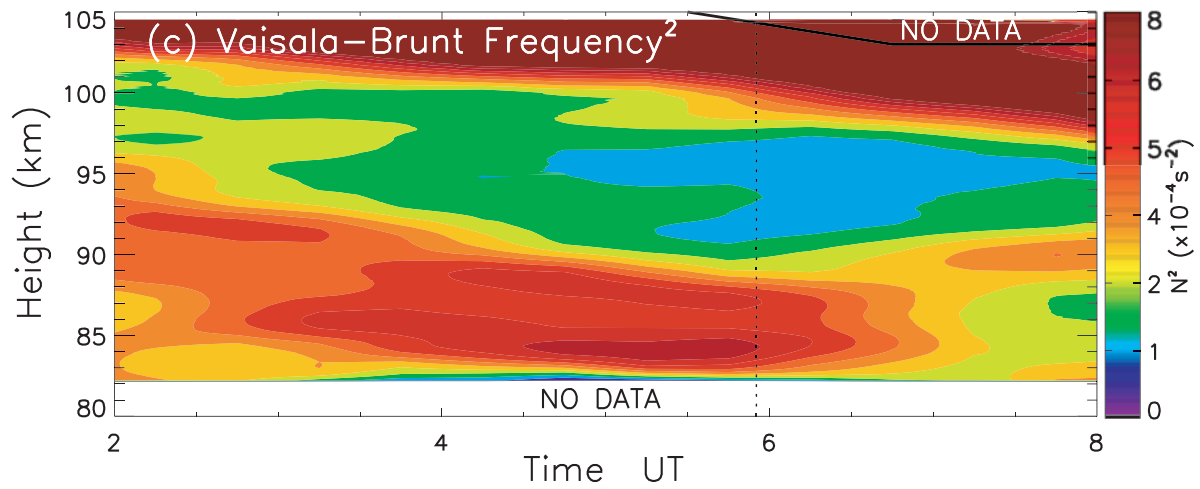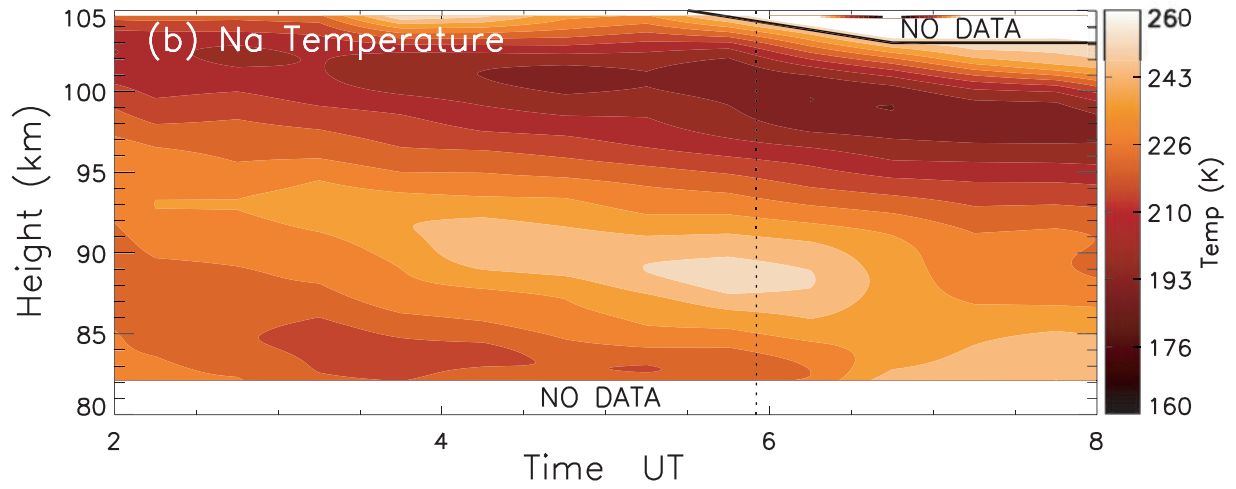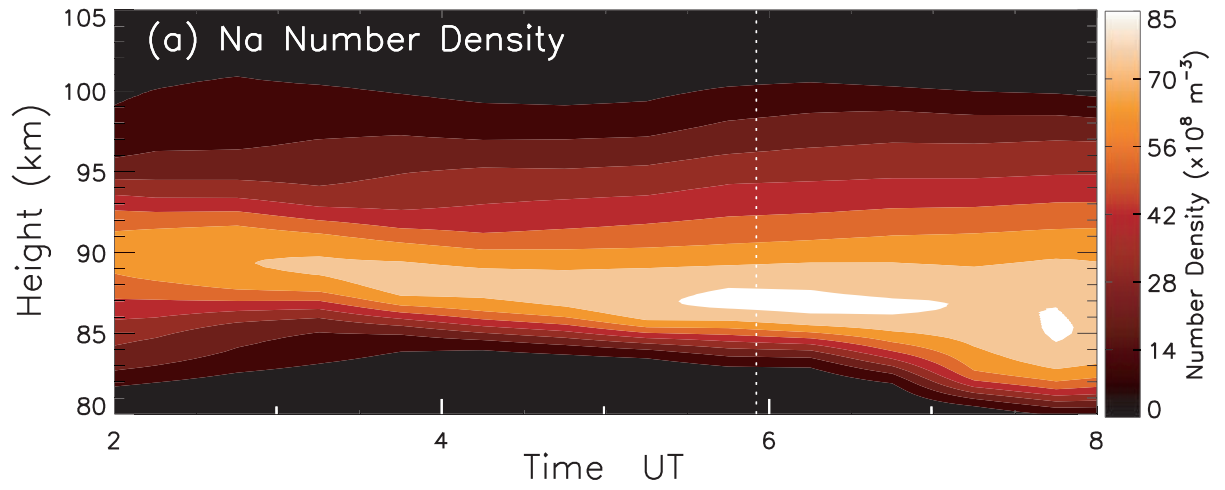
that the height of the temperature maximum in Figure 12b occurred along the top boundary (3–4 km above the center) of the ducting region and both moved downward together until about 0630 UT after which time they disappeared.

[35] Local winds can enhance or reduce the effectiveness of a preexisting thermally induced ducting region, such as in Figure 12c, depending on the relative directions of the wind and the wave propagation. Anti-parallel winds and wave azimuths will lead to an enhancement of the duct whereas co-parallel azimuths will reduce the duct's effectiveness [*Jones*, 1972]. In addition, a wind shear can also create ducting conditions in the absence of a thermal inversion layer. For these reasons, and because no mesospheric wind measurements were made at Fort Collins on 14 November, Figure 12c may not represent exactly the ducting conditions existing above Ft. Collins. In fact, the ducting region was probably more pronounced than that shown because the lowest N^2 values (blue contoured region in Figure 12c) were very close to zero (but positive). The disappearance of the thermal duct after about 0630 UT was due possibly to changes in the wind and temperature field brought about by the disturbance.

[36] Using the lidar data from Ft Collins on 14 November and the *Dewan and Picard* [1998] model equations presented in section 2, we will estimate several parameters of the bore. The temperature inversion was centered near 86 km and had a width (FWHM) of 6 km, so $h_0 = 3$ km. Using data from the *National Oceanic and Atmospheric Administration*'s [1976]*U.S. Standard Atmosphere, 1976*, g' was calculated to be 0.91 ms^{-2}. The details of this method are described more fully in *Dewan and Picard* [1998]. For a nonturbulent undular bore, $\beta < 0.3$. So, setting an upper limit of $\beta = 0.3$ and using equation (1), we find $h_1 = 3.9$ km. Equations (2) and (3) yielded values for U and λ_h of 72 ms^{-1} and 21 km, respectively. The estimate values match very well the observed values of U = 60.2 ms^{-1} and $\lambda_h = 30.2$ km. Equation (4) estimated the bore amplitude, a, to be 0.68 km.

[37] We can also use the assumption that an altitude increase of 1 km results in an adiabatic temperature increase of 10 K [*Makhlouf et al.*, 1990]. The OH temperature data from the SOR shows a 5 K increase during the event (Figure 9b) indicating a decrease in height of 0.5 km. So, $h_1 = h_0 - 0.5 = 3.5$ km. In that case, $\beta = 0.17$ from equation (2). Equations (3) and (4) yielded values of U = 66 ms^{-1} and $\lambda_h = 25$ km, respectively. The amplitude estimate from equation (4) was a = 0.34 km. These model estimates also agree very well with the measured values above and provide further evidence that the disturbance was the result of an undular

bore propagating on a stable inversion layer and not merely a large ducted internal gravity wave. Notably also, because the speed of the bore is dependent on the width of the stable layer, the constancy of the observed speed of the bore over the course of its lifetime over MDO indicates that the vertical thickness of the temperature inversion was remarkably constant over a very large horizontal distance (∼1000 km).

[38] A stable inversion layer is necessary for a bore disturbance to propagate, so its presence above Fort Collins, would provide the bore with a means of propagation southward through the mesosphere. Inversion layers in the upper mesosphere, also known as mesospheric inversion layers (MIL's), are known to be stable and long-lasting [*Meriwether and Gardner*, 2000]. *Hauchecorne et al.* [1987] showed using simultaneous, spatially separated lidar measurements that MIL's can extend over distances of over 550 km. The deduced trajectory of the bore disturbance would suggest that their extent is much larger (∼1000–1500 km) and, combined with their stability, probably play an important role in the transport of wave energy over large distances.

[39] As mentioned earlier, it was not known whether a temperature inversion existed over MDO or the SOR during the time of the bore, but the SOR radar wind data indicated that a large meridional wind shear occurred just before the appearance of the wave train (Figure 11a). Although it has never been shown, either experimentally or theoretically, that a Doppler duct generated by a wind shear, we could speculate that it is possible.

6. Energy Dissipation Within a Bore

[40] A bore disturbance dissipates energy by creating a series of trailing wavefronts phase-locked to the disturbance. The rate of addition of waves to the back of the wave train is an indicator of the rate of dissipation by the bore and also of its lifetime. *Dewan and Picard* [1998] estimated the rate of addition of waves to the train by the bore to be

$$\frac{dW}{dt} = 1.8 \times 10^3 \frac{U(h_1 - h_0)^3}{2a^2 \lambda_h h_1} \quad (hour^{-1}) \qquad (7)$$

[41] The time history of the number of light and dark wavefronts visible in each 557.7 nm image during the 14 November event is plotted in Figure 13a with the light/dark wavefronts represented as open/filled circles. A linear increase in the number of light and dark wavefronts is clearly seen in Figure 13a. The line of best fit is shown as a dark line and corresponds to an increase of 6.2 ± 0.5 hour^{-1}.

Figure 12. (opposite) Measured and deduced parameters from the CSU lidar at Ft. Collins, CO. on 14 November, 1999. (a) Contour plot of the time history of the mesospheric Na density profile. A 20% enhancement occurred around 0600 UT, which coincided with the deduced passage of the wave disturbance over the site. The enhancement disappeared after 1–2 hours. (b) Contour plot of 30-minute mean temperature profiles of the mesospheric Na layer. A large 50 K temperature inversion in the 85–90 km height region can be seen propagating downward at 0.4 ms^{-1} during the night. The vertical line denotes the deduced time of passage of the bore disturbance over Ft. Collins. The center of the temperature inversion layer occurred at 88.6 km at 0600 UT. (c). Contour plot of the square of the Brunt-Vaisala frequency (in units of $\times 10^{-4}$s^{-2}) deduced from the temperature profiles in Figure 12b. A 6-km wide ducting region, resulting from the inversion layer, is centered near 86 km (contours in red). The regions of reduced wave propagation are colored blue. The height and time of occurrence of the ducting region are consistent with the imaging measurements at MDO and SOR and suggest a possible connection between the temperature inversion and the subsequent wave event observed 1100 km to the south at MDO. The deduced values below 82 km are considered unreliable.
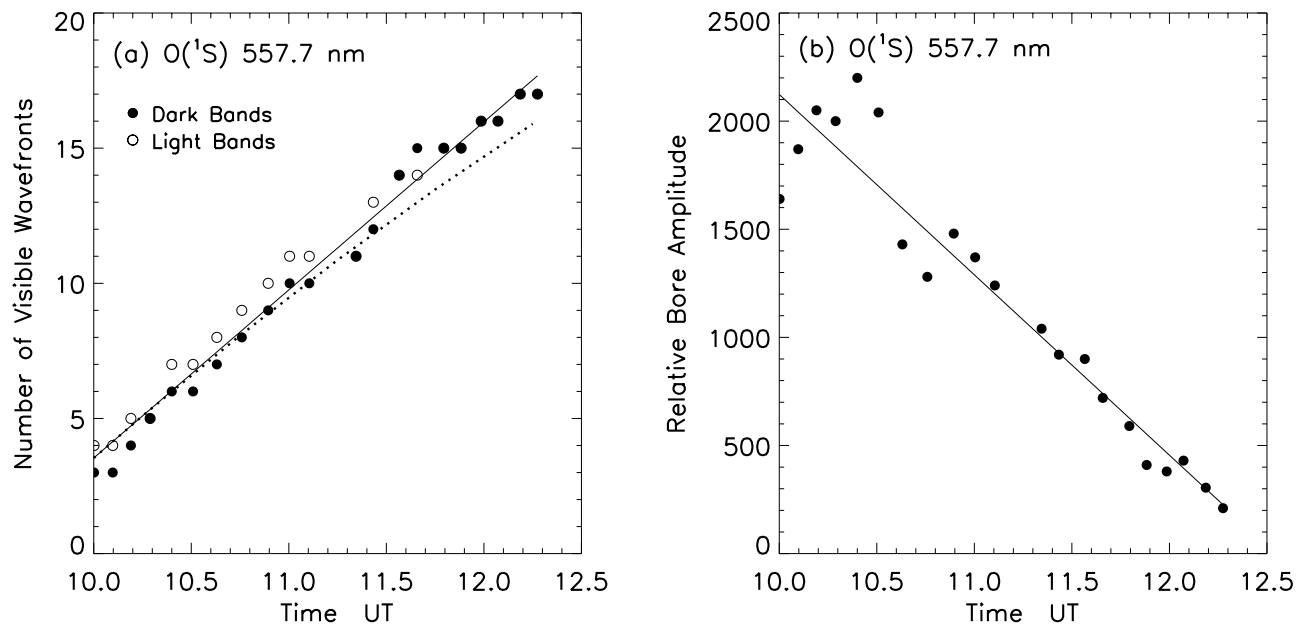
Figure 13. (a) Time history of the number of light (open circles) and dark (filled circles) wavefronts during night of 14 November 1999. The solid line is the best linear fit to the data. The dotted curve is the estimated variation of the number of wavefronts given the observed velocity variation along the wave train. (b) Time history of the amplitude of the leading wave disturbance in the 557.7 nm emission during the night. Specifically, it is the difference between the brightness level of the emission enhancement just prior to the wave train (clearly seen in Figure 7) and the leading dark wavefront. The variation is clearly linear over time, indicating that the bore disturbance and the wave train were dissipating energy.

The end of the train appeared to occur toward the north, approximately 15° above the horizon, at about the altitude of the summit of Mt. Locke (see Figure 4). Clear sky at an elevation lower than and to the west of the summit indicated that the waves were not visible there. However, the integrated line-of-sight distance through a 10-km wide 557.7 nm $O(^1S)$ layer at an elevation of 15° is 38 km so, at lower elevations the bore waves, whose phase fronts were vertical, may not be detected because of the viewing geometry. Even though Figure 8a shows that the elevation of the lowest visible wavefronts increased during the event it was not certain that the last wavefront in each image corresponded to the end of the wave train. Because of this uncertainty, we used the observed speeds of the individual wavefronts along the train (Figure 8b) to estimate the time history of the number of wavefronts, with the assumption that none were added or removed during the period of the event but merely became visible over the horizon, or over a certain viewing angle. Using that assumption, and because the individual wavefronts each traveled at different speeds, the rate of increase of visible wavefronts should decrease over time because the following wavefronts would take longer to appear (since they are traveling progressively slower).

[42] The estimated time history is shown as a dotted curve in Figure 13a. If all wavefronts moved at the same speed the time history would be linear. The difference between the estimated (dotted) and the observed (solid) time histories of the number of visible wavefronts provided an estimate of the number of waves added by the disturbance. The measurements indicated that 1.0 ± 0.8 waves hour^{-1} were added. Using equation (7) and the deduced parameters in the preceding section, we obtain an estimated wave addition

rate of 2.5 hour^{-1} for $h_1 = 3.9$ km, and 1.5 hour^{-1} for $h_1 = 3.5$ km. The observed and estimated wave addition rates are very similar, especially for the $h_1 = 3.5$ km case. For comparison, the model estimate of the wave addition rate for the *Taylor et al.* [1995a] event was 2.8 hour^{-1} [*Dewan and Picard*, 1998] but no estimate from the observations was possible.

[43] The model estimates obtained for the wave addition rate, and for the phase speed and horizontal wavelength in the preceding section, suggest that a value of $h_1 = 3.5$ km clearly provides a better estimate of the observed values than $h_1 = 3.9$ km. Recall, that for the latter case we obtained a value for h_1 by setting β to 0.3 as an estimated upper limit of an undular bore. The value of $h_1 = 3.5$ km was inferred from the OH temperature mapper measurements at the SOR and using the adiabatic decrease in temperature with height.

[44] The brightness amplitude of the wavefronts decreased over time, which indicated that the bore was dissipating energy. Figure 13b shows the difference between the brightness level of the 557.7 nm emission enhancement just prior to the wave train (clearly seen in the Figure 7) and the leading dark wavefront. This represents the amplitude of the bore disturbance and it clearly decreases linearly with time, indicating that the bore was dissipating energy at constant rate. Furthermore, the width of the leading dark wavefront (see Figure 10a) increased with time along the direction of propagation indicating that the wavefront was undergoing dispersion.

7. Origin of Disturbance

[45] Meteorological disturbances, such as convective activity, have been suggested as one source of mesospheric
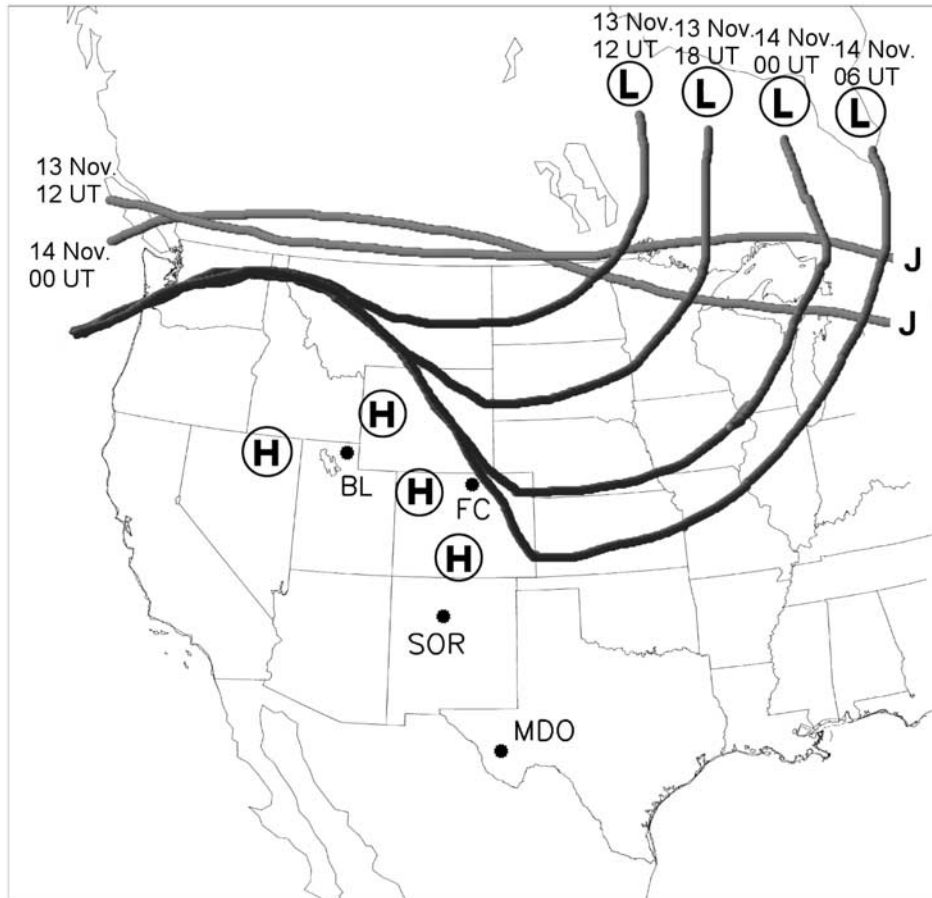
Figure 14. Map showing the six-hourly time evolution of a large cold front, that was situated over the continental United States, during 13–14 November 1999. A deep depression (denoted by L) lay over northeastern Canada. A group of high-pressure zones (denoted by H's) over the western United States blocked the movement of the front into the southwest. During the same period, the polar jet stream at the 250 mB level (∼10.5 km altitude) (denoted by J) lay along the US/Canadian border.

gravity wave activity at low and middle latitudes [*Taylor and Hapgood*, 1988; *Taylor et al.*, 1995b; *Dewan et al.*, 1998]. Auroral activity may also contribute at high latitudes. Gravity waves propagating into the mesosphere can interact and deposit their energy and momentum into the mean wind flow, called critical-level interaction. *Huang et al.* [1998] presented observational evidence of a gravity-wave undergoing critical-level interaction and producing a large temperature inversion layer due to heating by the unstable wave. *Dewan and Picard* [2001] have suggested that mesospheric bores may form by a similar process involving a critical-level interaction between a large gravity wave and the mean wind.

[46] During the 24 hours prior to the event's appearance, a large cold front, initially aligned east to west and similar to the disturbance's wavefront alignment, formed over the northern US and southern Canada (see Figure 14). The front moved southward during this time and reached Colorado at around 0000 UT on 14 November. The front's alignment and location during the hours prior to the appearance of the wave suggests that it may have been responsible for the generation of the disturbance. An all-sky imager at

Bear Lake Observatory (BLO), Utah (41.9°N, 111.4°W), approximately 500 km west of Fort Collins (Figure 2), was operating during the same period as the other sites discussed earlier, but did not detect the disturbance. The reason may be due to the temporal evolution of the front as it moved southward. It skirted the eastern side of the Rocky Mountains because of a high pressure region situated there and its alignment direction became more NW to SE. The bore disturbance may have also been launched when the front was near the latitude of BLO, and so reached the upper atmosphere to the south of the site.

[47] The jet stream has been suggested as a possible source of gravity waves in the mesosphere [*Taylor and Hapgood*, 1988]. Prior to the event, the jet stream lay approximately 2000 km due north of the MDO site, extending along the US/Canada border. Since no evidence was seen of the disturbance in the Bear Lake images, the cold front is probably the more likely progenitor, however the jet-stream may have been partly responsible. A frontal origin was suggested for the *Swenson and Espy* [1995] "wall event". In that case, the disturbance was observed to propagate to the southeast, directly away from a large

Table 1. Three-Hour Magnetic K_p Indices Around the Times of the Various Wave Events Described in the Accompanying Text[a]

Date	Time, UT						Event
	0–3	3–6	6–9	9–12	12–15	15–18	
9 Oct. 1993	3^0	6^-	$\mathbf{5^+}$	$\mathbf{7^-}$	4^0	3^+	*Swenson and Epsy* [1995]
10 Oct. 1993	4^0	5^0	4^+	$\mathbf{4^0}$	$\mathbf{5^-}$	3^-	*Taylor et al.* [1995a]
14 Nov. 1999	3^-	2^+	$\mathbf{3^-}$	$\mathbf{2^0}$	3^-	3^-	This study

[a]The indices in bold denote the time periods of occurrence of each event.

tropospheric frontal system and the wavefronts were aligned roughly parallel to the front.

[48] Prior to the present event, the front lay to the north of the sites, but east of Bear Lake. Although speculative, the front may have created large amounts of wave activity which propagated into the mesosphere, interacting with the local medium and producing the temperature inversion layer [*Hauchecorne et al.*, 1987; *Huang et al.*, 1998]. The jet stream may have also provided wave energy which propagated southward through the previously created ducting region.

[49] There was no clear evidence of an auroral origin for this disturbance. Firstly, there was no visible evidence of auroral activity in any of the images. Images from the NASA Polar satellite showed a relatively quiescent auroral oval during the 6 to 12 hours prior to the event. A stable auroral red (SAR) arc, but no diffuse aurora, was visible in 630.0 nm emission all-sky images at Millstone Hill, Massachusetts (42.6°N, 71.5°W). Table 1 lists the K_p indices around the time of the event, as well as for the two other events in the literature. The indices during the period of the events are shown in bold. Approximately 12 hours prior to the appearance of the event at the SOR the K_p indices were 6^+ and 5^+, respectively, indicating moderate storm activity. During the 6 hours prior to, and during, the event the K_p indices were relatively low at about 3. The value of the indices did not indicate a level of activity expected to produce auroral effects at the latitude of MDO and the SOR (40 to 44°N geomag.). For this reason, and because no evidence of the disturbance was detected at Bear Lake, an auroral origin for the disturbance is considered to be unlikely. The level of geomagnetic activity prior to the two similar mesospheric wave events reported in the literature at low (~20°) latitude [*Taylor et al.*, 1995a; *Swenson and Espy*, 1995] (Table 1) further indicates that such wave disturbances occur independently of geomagnetic activity.

8. Discussion

[50] The wave event observed on 14 November 1999 at MDO appears to be the result of an internal undular bore propagating in the mesosphere. Mesospheric bores have been reported only rarely [*Taylor et al.*, 1995a]. The present event is particularly interesting because of its large intrinsic brightness and the availability of simultaneous imaging, wind and temperature data from several, widely spaced sites. This event, and the *Taylor et al.* [1995a] event, exhibited similar characteristics: a sudden onset of a long wave train which continued for several hours. Moreover, both events exhibited a complementarity in the brightnesses

between the emission layers from different height regions, although that may not occur in all cases. The present event exhibited greater nonlinear behavior than the *Taylor et al.* [1995a] event with the wavefronts acting more like a train of independent solitons propagating on top of a stable layer.

[51] The quasi-monochromatic gravity waves that are frequently observed with all-sky imaging systems usually exhibit either (i) no phase variation between emission layers if they are ducted or evanescent, or (ii) they exhibit a phase variation between the imaged emission layers if they are freely propagating. A freely propagating gravity wave may, however, produce a complementary pattern between different emission layers if the vertical wavelength of a gravity wave is a half-integral multiple of the height separation between the layers.

[52] The complementarity brightness variations observed in the three emissions at MDO indicated that the bore was centered near 86–87 km, below the $O(^1S)$ and Na layers but above the OH layer. The precise centroid altitudes of these emissions was unknown but they usually occur near 96 km ($O(^1S)$) and 90 km (Na) and 87 km (OH), as shown in Figure 1c. As the disturbance moved through the region it caused each layer to increase (decrease) in height and so produce a decrease (increase) in the emission rate. Figure 1a shows schematically how a bore disturbance would cause the top and bottom boundaries of a duct to oscillate 180° out of phase. As a result, the higher Na and $O(^1S)$ layers would exhibit a wave pattern complementary to the lower OH layer.

[53] During the passage of the waves, the mean zenith Na emission brightness at MDO increased but the $O(^1S)$ emission brightness decreased (see Figure 6), even though the small-scale wavefronts in both emissions were in phase (but 180° out of phase with the OH wavefronts (see Figure 7)). Furthermore, the SOR Temperature Mapper data showed the OH zenith intensity time history (Figure 9a) had a similar form to the Na time history at MDO (Figure 6). The most likely reason for the Na intensity enhancement after the bore's passage was because the temperature increased by 4–5 K after the passage of the disturbance (the OH measurements in Figure 9b) at the SOR and, since the Na emission rate is more temperature sensitive than the $O(^1S)$ emission rate, the Na emission was enhanced.

[54] As indicated earlier, the propagation direction of the disturbance varied by about 30° in a clockwise direction between 7–12 UT. During the same period, the 2-hourly mean radar wind vectors in the 94 and 98 km height region were directed in the opposite direction to the disturbance's motion and also varied clockwise, by about 90°, due to diurnal tidal motion. This suggest that the diurnal tide contributed in blocking the southward propagation of the disturbance.

9. Conclusion

[55] A bright wave event which was observed with all-sky imaging systems in three nighttime mesospheric emissions on 14 November 1999 at two sites in the southwestern United States separated by over 500 km. The event was characterized by a frontal onset of a series of extensive wavefronts which propagated southward across the entire sky. The wavefronts were observed at three different wave-

lengths and exhibited a complementarity in the intensity of the wave structure between the $O(^1S)$/Na and OH emissions. The waves were also easily visible to the naked eye at MDO and the entire event lasted at least 5 $\frac{1}{2}$ hours at both sites.

[56] We propose that the disturbance was due to an internal undular bore propagating within a ~6-km wide (FWHM) ducting region near 86 km. The event differed from a large-amplitude gravity wave [*Swenson and Espy*, 1995; *Swenson et al.*, 1998] in several ways, the most important being that each wavefront behaved like a single nonlinear solitary wave (or soliton) propagating independently of the others; the leading wavefronts propagating faster than the trailing wavefronts. In addition, there was excellent agreement between the measured speed of the bore and a theoretical estimate [*Dewan and Picard*, 1998] determined from the width of the stable ducting region. The event was also similar to the case study by *Dewan and Picard* [1998] of the *Taylor et al.* [1995a] event but the latter event did not exhibit the degree of nonlinear behavior just mentioned.

[57] Lidar observations made approximately 1100 km to the north of MDO, showed evidence of a large inversion layer occurring in the 85−90 km height region during the same night. Depending on the time of its formation, the disturbance would have passed over the lidar site around the time when the inversion was largest and when it provided the best conditions for ducted propagation. Furthermore, horizontal wind measurements at the SOR during the time of the disturbance exhibited a very strong wind shear in the propagation direction of the bore, also indicating a ducting region may have also been present there. The combined optical and radar measurements provided strong evidence that inversion layers with horizontal scale-sizes of ~1000−1500 km can exist, allowing large wave disturbances in the mesosphere to propagate over large distances on time-scales of several hours. The bore disturbance most probably originated from a large tropospheric frontal system, aligned east to west, which had developed over northern Canada and moved southward over the United States.

References

Armstrong, E. B., The association of visible airglow features with a gravity wave, *J. Atmos. Terr. Phys.*, 44, 325–366, 1982.

Bates, D. R., Bright nights, in *Physics of the Upper Atmosphere*, edited by J. A. Ratcliffe, pp. 236–237, Academic, San Diego, Calif., 1960.

Baumgardner, J., B. Flynn, and M. Mendillo, Monochromatic imaging instrumentation for applications in aeronomy of the Earth and planets, *Opt. Eng.*, 32(12), 3028–3032, 1993.

Bore Riders Club, http://www.boreriders.com, 2001.

Christie, D. R., Long nonlinear waves in the lower atmosphere, *J. Atmos. Sci.*, 46, 1462–1491, 1989.

Clarke, R. H., R. K. Smith, and D. G. Reid, The morning glory of the Gulf of Carpenteria: An atmospheric undular bore, *Mon. Weather Rev.*, 109, 1726–1750, 1981.

Dewan, E. M., and R. H. Picard, Mesospheric bores, *J. Geophys. Res.*, 103, 6295–6305, 1998.

Dewan, E. M., and R. H. Picard, The origin of mesospheric bores, *J. Geophys. Res.*, 106, 2921–2927, 2001.

Dewan, E. M., R. H. Picard, R. R. O'Neil, H. A. Gardiner, J. Gibson, J. D. Mill, E. Richards, M. Kendra, and W. O. Gallery, MSX satellite observations of thunderstorm-generated gravity waves in mid-wave infrared images of the upper stratosphere, *Geophys. Res. Lett.*, 25, 939–942, 1998.

Donahue, T. M., B. Guenther, and R. J. Thomas, The distribution of atomic oxygen in the upper atmosphere deduced from OGO-6 airglow observations, *J. Geophys. Res.*, 78, 6662–6689, 1973.

Drazin, D. G., and R. S. Johnson, *Solitons: An Introduction*, 226 pp., Cambridge Univ. Press, New York, 1989.

Eska, V., J. Hffner, and U. von Zahn, The upper atmosphere potassium layer and its seasonal variations at 54°N, *J. Geophys. Res.*, 103, 29,207–29,214, 1998.

Hauchecorne, A., M. L. Chanin, and R. Wilson, Mesospheric temperature inversion and gravity wave breaking, *Geophys. Res. Lett.*, 14, 933–936, 1987.

Hocking, W. K., B. Fuller, and B. Vandepeer, Real-time determination of meteor-related parameters utilizing modern digital technology, *J. Atmos. Sol. Terr. Phys.*, 23, 155–169, 2001.

Huang, T. Y., H. Hur, T. F. Tuan, X. Li, E. M. Dewan, and R. H. Picard, Sudden narrow temperature-inversion-layer formation in ALOHA-93 as a critical-layer-interaction phenomenon, *J. Geophys. Res.*, 103, 6323–6332, 1998.

Isler, J. R., M. J. Taylor, and D. C. Fritts, Observational evidence of wave ducting and evanescence in the mesosphere, *J. Geophys. Res.*, 102, 26,301–26,313, 1997.

Jones, W. L., Ducting of internal gravity waves on a stable layer with a shear, *J. Geophys. Res.*, 77, 3879–3885, 1972.

Lamb, H., *Hydrodynamics*, 6th ed., Dover, Mineola, N. Y., 1932.

Lighthill, M. J., *Waves in Fluids*, 504 pp., Cambridge Univ. Press, New York, 1978.

Mahapatra, P. R., R. J. Doviak, and D. S. Zrnic, Multisensor observation of an atmospheric undular bore, *Bull. Am. Meteorol. Soc.*, 72, 1468–1480, 1991.

Makhlouf, U., E. Dewan, J. R. Isler, and T. F. Tuan, On the importance of the purely gravitationally induced density, pressure, and temperature variation in gravity waves: Their application to airglow observations, *J. Geophys. Res.*, 95, 4103–4111, 1990.

Meriwether, J., and C. S. Gardner, A review of the mesospheric inversion layer phenomenon, *J. Geophys. Res.*, 105, 12,405–12,416, 2000.

Munasinghe, G., H. Hur, T. Y. Huang, A. Bhattachryya, and T. F. Tuan, Application of the dispersion formula to long- and short-period gravity waves: Comparisons with ALOHA-93 data and an analytical model, *J. Geophys. Res.*, 103, 6467–6481, 1998.

National Oceanic and Atmospheric Administration, *U.S. Standard Atmosphere, 1976*, U.S. Gov. Print. Off., Washington, D.C., 1976.

Newman, A. L., Nighttime Na D emission observed from a polar-orbiting DMSP satellite, *J. Geophys. Res.*, 93, 4067–4075, 1988.

Peterson, A. W., Airglow events visible to the naked eye, *Appl. Opt.*, 18, 3390–3393, 1979.

Rayleigh, L., Note on tidal bores, *Proc. R. Soc. London, Ser. A*, 5, 495, 1908.

She, C. Y., J. R. Yu, J. W. Huang, C. Nagasawa, and C. S. Gardner, Na temperature lidar measurements of gravity wave perturbations of wind, density, and temperature in the mesopause region, *Geophys. Res. Lett.*, 18, 1329–1331, 1991.

Simpson, J. E., *Gravity Currents: In the Environment and the Laboratory*, Ellis Horwood Series in Environmental Science, 244 pp., Ellis Horwood, Chichester, England, 1987.

Slanger, T. G., and D. E. Osterbrock, Investigations of potassium, lithium, and sodium emission in the nightglow and OH cross-calibration, *J. Geophys. Res.*, 105, 1425–1429, 2000.

Smith, R. K., Traveling waves and bores in the lower atmosphere: The 'Morning Glory' and related phenomena, *Earth Sci. Rev.*, 25, 267–290, 1988.

Smith, S. M., M. Mendillo, J. Baumgardner, and R. R. Clarke, Gravity wave imaging from a sub-auroral site: First results from Millstone Hill, *J. Geophys. Res.*, 105, 27,119–27,130, 2000.

Swenson, G. R., and P. J. Espy, Observations of two-dimensional airglow structure and Na density from the ALOHA, October 9, 1993, "storm flight", *Geophys. Res. Lett.*, 22, 2845–2848, 1995.

Swenson, G. R., and S. B. Mende, OH emission and gravity waves (including a breaking wave) in all-sky imagery from Bear Lake, UT, *Geophys. Res. Lett.*, *21*, 2239–2242, 1994.

Swenson, G. R., J. Qian, J. M. C. Plane, P. J. Espy, M. J. Taylor, D. N. Turnbull, and R. P. Lowe, Dynamical and chemical aspects of the mesospheric Na "wall" event on October 9, 1993 during the Airborne Lidar and Observations of Hawaiian Airglow (ALOHA) campaign, *J. Geophys. Res.*, *103*, 6361–6380, 1998.

Taylor, M. J., and M. A. Hapgood, Identification of a thunderstorm as a source of short period gravity waves in the upper atmosphere nightglow emissions, *Planet. Space Sci.*, *36*, 975–985, 1988.

Taylor, M. J., and M. J. Hill, Near infrared imaging of hydroxyl wave structure over an ocean site at low latitudes, *Geophys. Res. Lett.*, *18*, 1136–1333, 1991.

Taylor, M. J., M. A. Hapgood, and P. Rothwell, Observations of gravity wave propagation in the OI (557.7 nm), Na (589.2 nm) and the near infrared OH nightglow emissions, *Planet. Space Sci.*, *35*, 413–427, 1987.

Taylor, M. J., D. N. Turnbull, and R. P. Lowe, Spectrometric and imaging measurements of a spectacular gravity wave event observed during the ALOHA-93 campaign, *Geophys. Res. Lett.*, *22*, 2849–2852, 1995a.

Taylor, M. J., V. Taylor, and R. Edwards, An investigation of thunderstorms as a source of short period mesospheric gravity waves, in *The Upper Mesosphere and Lower Thermosphere: A Review of Experiment and Theory*, *Geophys. Monogr. Ser.*, vol. 87, pp. 177–184, AGU, Washington, D. C., 1995b.

Taylor, M. J., W. R. Pendleton, S. Clark, H. Takahashi, D. Gobbi, and R. A. Goldberg, Image measurements of short-period gravity wave at equatorial latitudes, *J. Geophys. Res.*, *102*, 26,283–26,299, 1997.

Taylor, M. J., W. R. Pendleton, C. S. Gardner, and R. J. States, Comparison of terdiurnal oscillations in mesospheric OH rotational temperature and Na lidar temperature measurements at mid-latitudes for fall/spring conditions, *Earth Planets Space*, *51*, 877–885, 1999.

Walterscheid, R. L., J. H. Hecht, R. A. Vincent, I. M. Reid, J. Woithe, and M. P. Hickey, Analysis and interpretation of airglow and radar observations of quasi-monochromatic gravity wave in the upper mesosphere and lower thermosphere over Adelaide (35°S, 138°E), *J. Terr. Sol. Atmos. Phys.*, *61*, 461–478, 1999.

Yu, J. R., and C.-Y. She, Climatology of a midlatitude mesopause region observed by a lidar at Fort Collins, Colorado (40.6°N, 105°W), *J. Geophys. Res.*, *100*, 7441–7452, 1995.

—————————————

J. Baumgardner, M. Mendillo, and S. M. Smith, Center for Space Physics, Boston University, Boston, MA 02215, USA. (smsm@bu.edu)

W. Hocking, Department of Physics and Astronomy, University of Western Ontario, London, Ontario, Canada, N6A 3K7.

C.-Y. She, Physics Department, Colorado State University, Fort Collins, CO 80523, USA.

G. R. Swenson, Department of Electrical and Computer Engineering, University of Illinois, Urbana, IL 61801-2307, USA.

M. J. Taylor, Space Dynamics Laboratory and Physics Department, Utah State University, Logan, UT 84322-4145, USA.